SOIL-STRUCTURE INTERACTION EFFECTS ON SEISMIC FRAGILITY CURVES OF STEEL MRF STRUCTURES

H. Masaeli[(1)], A. Beitollahi[(2)]

[(1)] *PhD Candidate, Amirkabir University of Technology (Tehran Polytechnic), Tehran, Iran, hamid_msli@aut.ac.ir*
[(2)] *Assistant Professor and Head of Earthquake Engineering & Engineering Seismology Department, Road Housing and Urban Development Research Center, Tehran, Iran, beitollahi@bhrc.ac.ir*

Abstract

Seismic loss estimation of structures rested on soil is inevitably influenced by soil-structure interaction (SSI). To evaluate this fact, the present study is focused on seismic damage assessment of low-rise steel moment resisting frames (MRFs) incorporating SSI effects. To this end, incremental dynamic analyses (IDAs) are performed using a suit of real ground motion records. A five-story MRF structure is selected as representative of building inventory in Iran. The structure is supported by single footings. To evaluate the SSI effects, four cases are compared including (i) fixed base, (ii) linear SSI and uncoupled footings (i.e. without tie beams), (iii) nonlinear SSI and uncoupled footings, and (iv) nonlinear SSI and coupled footings (i.e. with tie beams). The SSI effect is represented by modified Beam-on-nonlinear Winkler foundation (BNWF) model. An appropriate structural damage index based on summation of cumulative plastic hinges' rotations is employed. The seismic fragility curves of the structures are derived and compared for the above-mentioned cases. The results show that nonlinear SSI has significant effects on seismic fragility curves and consequently the overall amount of seismic loss estimation. Evidently, these effects are mitigating especially in case of footings with tie beams. However, some adverse displacements (i.e. foundation uplifting) are expected in case of footings without tie beams through which the local instabilities would be probable during the excitation period. As another consequence, excessive residual foundation tilting especially in exterior footings could lead to serious problems in serviceability of the structure after a strong event. Overall, based on findings of this study, the obtained modified fragility curves are supposed to be helpful for the earthquake engineers to conduct more realistic loss estimations considering SSI effects. These modification factors need to be generalized with respect to a variety of structural systems, site types and foundation configurations.

Keywords: Soil-structure interaction, seismic fragility curve, earthquake loss estimation, steel moment-resisting frame

1. Introduction

One of the pillars of earthquake preparedness is to provide a seismic loss estimation platform in order to predict the consequences of an uncertain earthquake to civil infrastructure. Application of fragility curves is known as a solution to overcome the highly unpredictable nature of the problem in seismic hazard programs. Fragility is a term that describes the probability of failure to meet a performance objective as a function of demand on the system. The earliest widespread application of fragility analysis against earthquake demands was provided in ATC-13 [1]. The well-known program for loss estimation, HAZUS [2], developed under Federal Emergency Management Agency (FEMA) sponsorship, incorporates fragilities for 36 categories of building and four damage states. Both ATC-13 and HAZUS are based to a great extent on engineering judgments.

More recent approaches have relied more on computational bases. In the new paradigm of consequence-based risk management (CBRM) performance assessment tools are being developed for use in seismic risk reduction. The fragility of components or systems is a key element of this process, as it not only defines the probability of reaching target damage states as a function of a specified measure of earthquake ground motion intensity but also is required for estimating expected or maximum probable losses.

Several studies [e.g. 3-5] in the literature are devoted to seismic fragilities of several typical low-to-mid-rise steel and reinforced concrete buildings representative of design and construction practices. A comparison of these fragilities, based on nonlinear time history analyses (NTHAs), with those incorporated in HAZUS indicates that the fragilities from HAZUS tend to be quite conservative in predicting collapse in comparison with those computed through a more sophisticated NTHA-based assessment, particularly for the steel frames. Accordingly, the drift limits implied in the HAZUS fragilities are conservative (4-5% in HAZUS vs 9-10% from NTHAs [5]), and the logarithmic standard deviations are substantially higher, often exceeding 90%, while those from NTHAs are on the order of 50% or less [5]. However, it should be noted that HAZUS is aimed at regional loss estimation rather than building-specific vulnerability assessment, and the large logarithmic standard deviations are due to considerable variation on construction details within each building category.

In general, fragility curves can include several sources of uncertainties: in the seismic loading, the soil site and the structural parameters defining the system. From a modern fragility modeling perspective, there is increasing demands for the analysis of epistemic uncertainties. In contrast, the notions of building fragility and vulnerability assessment, in current form, are not well established dealing with dynamic soil-structure interaction (SSI) effects, as one of the sources of uncertainties. To fill this gap and achieve more reliable loss estimation, there have been some attempts recently to develop the fragility modeling of the buildings incorporating SSI effects (e.g. [6]).

As a step toward considering SSI effect, Saez et al. [6] have studied the influence of nonlinear SSI on the seismic vulnerability assessment of a typical building with surface raft foundation. The seismic vulnerability was evaluated in terms of analytical fragility curves constructed on the basis of NTHAs. The developed fragility curves were compared with reference curves in HAZUS. Concerning the effect of the nonlinear SSI, a general reduction of seismic demand was found in the derived fragility curve. Saez et al. have postulated that the observed reduction in seismic demands can be associated fundamentally to two phenomena: radiation damping and hysteretic damping due to nonlinear soil behavior. They also explained that however, inelastic SSI could increase or decrease the seismic demand depending on the type of structure, the input motion characteristics and the dynamic soil characteristics. Overall, the main drawback of their study is neglecting the inelastic behavior within superstructure domain. That is why they had no choice but to limit their investigations to slight-to-moderate damage states. Consequently, they could not make observations of structural fragilities prior to collapse.

This study is mainly focused on seismic damage assessment of low-rise steel moment resisting frames (MRFs) while SSI effects are included. The inelastic behavior of superstructure is considered and consequently higher damage states can be evaluated. A five-story MRF structure is selected as representative of building inventory in Iran. The structure is supported by single footings. The SSI effect is represented by modified Beam-on-nonlinear Winkler foundation (BNWF) model. Incremental dynamic analyses (IDAs) are performed using a suit of real ground motion records. An appropriate structural damage index based on summation of cumulative plastic hinges' rotations is employed. The seismic fragility curves of the structures are derived and compared for different SSI conditions. The four comparative SSI conditions are including fixed base, linear SSI, and nonlinear SSI (i.e. foundation uplifting and soil yielding are considered). The foundation system in nonlinear SSI condition is supposed to be with or without tie beams.

2. Superstructure description

A 5-story steel frame is selected from three-dimensional structural modeling in which, to avoid the effects of geometrical asymmetry, plans are considered symmetric and similar. As depicted in Fig. 1a, each frame constitutes of three identical spans, and story height in all of them is 3.2 m. The width of spans is 6.0 m and the aspect ratio of the frame is then 0.89. Lateral seismic resisting system is special steel moment-resisting frame. For loading of structures, ASCE7-10 [7] is considered and the design dead and live loads are 550 and 200 kg/m^2, respectively. These gravity loads are distributed over the floor using a chessboard loading pattern. Structures are designed in fixed-base condition in accordance with the American Institute of Steel Construction AISC-05 [8]. Linear static and linear spectrum methods are employed for designing the frames using commercial software.

Steel profiles are all A36 with yielding strength of 2500 kg/cm^2, ultimate strength of 4070 kg/cm^2 and elasticity modulus of 2,100,000 kg/cm^2. Its Poisson's ratio is 0.3 and its density is equal to 7833 kg/cm^3. Loading assumptions required in the ASCE7-10 are as follows. Seismic zone is assumed to be zone 4, which includes the near-fault effects. Soil type is considered stiff soil (SD) (as per the code's instructions, we can assume the soil type to be SD when no information is available). Occupancy factor (I = IP) is considered 1. Moreover, 0.2 and 1 s spectral response accelerations (S_s and S_1) are considered 1.5 and 0.6, respectively. Thus, values of site coefficients (F_a and F_v) will be 1 and 1.5. Table 1 shows the section properties of the designed members as well as first- and second-mode periods of the constructed fixed-base model.

Table 1 – Section properties of the designed MRF structure and modal periods

Story	Sections		Modal periods	
	Column	Beam	T1 (s)	T2 (s)
1-5	HEB 320	IPE 360	1.35	0.41

Once the frame sections are designed assuming fixed-base superstructure, it is aimed to assess seismic performance of the soil-foundation-structure system in this study. The open-source program OpenSees [9] being developed in the Pacific Earthquake Engineering Research (PEER) Center is used to model the frame for NTHAs. The nonlinear behavior is represented using the concentrated plasticity concept with rotational springs. The rotational behavior of the plastic regions follows a bilinear hysteretic response based on the Modified Ibarra-Krawinkler Deterioration Model [10,11]. The bilinear steel behavior is assumed with secondary stiffness equal to 3%. A leaning column carrying gravity loads is linked to the frame to simulate P-Delta effects. Also, Rayleigh damping model was used, in which the damping ratio was assumed to be 2% of the critical damping for the first and fourth modes.

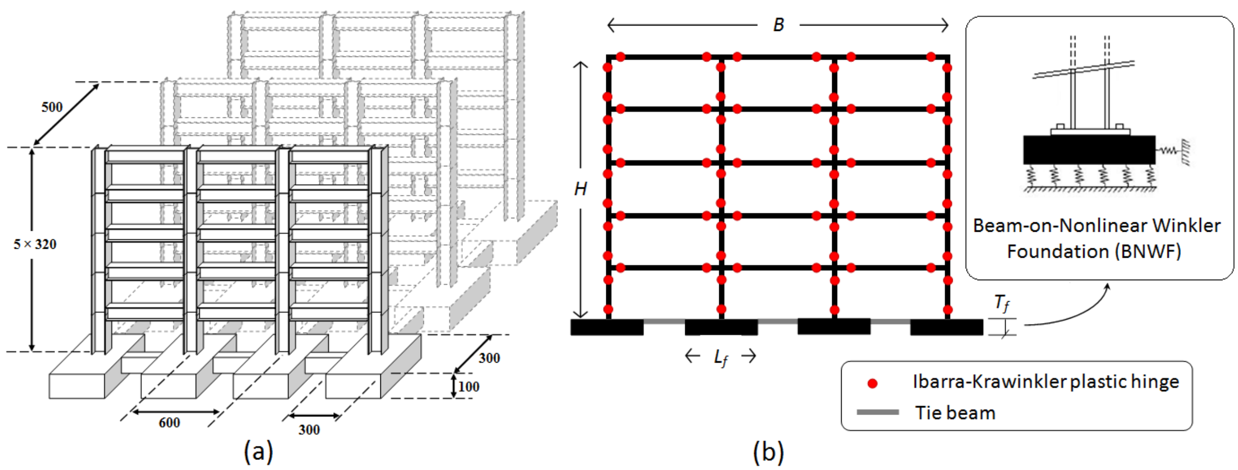

Fig. 1 – a) 3D view of the primary building-foundation system; b) Soil-foundation-structure model

3. Soil-foundation modeling

The beam-on-nonlinear-Winkler foundation (BNWF) model is used in this study to simulate nonlinear soil-foundation interaction. This model was proposed by Gajan et al. [12] and earlier by Harden and Hutchinson [13] and Harden et al. [14]. The BNWF model is also integrated with the openly available software platform OpenSees [9] by Raychowdhury and Hutchinson [15]. BNWF model with nonlinear springs of variable stiffness intensity can characterize the nonlinear, time dependent behavior of the foundation-soil interface for shallow foundations (footings, mats). These composite nonlinear springs, representing the underlying soil, are schematically displayed in Fig. 1b.

The BNWF model integrated with OpenSees, namely “ShallowFoundationGen” module, consists of elastic beam-column elements that capture the structural behavior of foundation as well as independent zero-length soil elements to model the soil-foundation interaction. Further details on BNWF model are available in PEER Report 2007/04 [16]. The parameters required for the BNWF model are related to soil and footing properties in addition to finite element mesh properties. Parameters of particular interest describing geotechnical properties of the subsoil are set corresponding to soil type III in accordance with Iranian seismic code, Standard 2800 (corresponding to soil type D based on site classification introduced in ASCE7-10).

Three comparative SSI conditions are considered in this study: first, “fixed-base” condition that means the foundation system and supporting soil are rigid; second, “linear SSI” condition, that means flexible foundation and soil but not allowed to uplift and no soil yielding; third, “nonlinear SSI” condition in which foundation uplifting and soil plasticity are included.

4. Input ground motion

The seismic performance of the soil-foundation-structure system is investigated through nonlinear dynamic time history analyses. An ensemble of 27 real accelerograms is used as a subset of near-field as well as far-field records recommended by FEMA-P695 [17]. Fig. 2 illustrates the ground acceleration histories of the selected ensemble. Of the entire 27 accelerograms, twelve records are classified as near-field pulselike, as judged by wavelet analysis classification [18], eight are classified as near-field no-pulse records, and the remaining seven are classified as far-field records.

To assess the effects of ground motion intensity, the suite of near-field records used in this study is scaled with respect to design spectrum introduced in Iranian seismic code, Standard 2800 [19]. The Standard 2800 guidelines define two levels of earthquake shaking hazard, termed Design Basis Earthquake (DBE) and Maximum Credible Earthquake (MCE). DBE is defined as a ground shaking with 10% probability of being exceeded in 50 years. MCE ground shaking has 2% probability of being exceeded in 50 years. Earthquake shaking demand on buildings is characterized by acceleration response spectra for these two hazard levels.

Ground motion record scaling is performed as recommended in FEMA-p695 [17]. Accordingly, record scaling involves two steps. First, individual records in each set are normalized by their respective peak ground velocities (PGVs). This step is intended to remove unwarranted variability between records due to inherent differences in event magnitude, distance to source, source type and site conditions, without eliminating overall record-to-record variability. In this study, the selected record set is normalized so that PGV is set equal to 50 cm/s. The ground acceleration histories of the normalized records are depicted in Fig. 2. Second, the normalized ground motions are collectively scaled to a specific ground motion intensity such that the median spectral acceleration of the record set matches the spectral acceleration at the fundamental period, T, of the index archetype that is being analyzed.

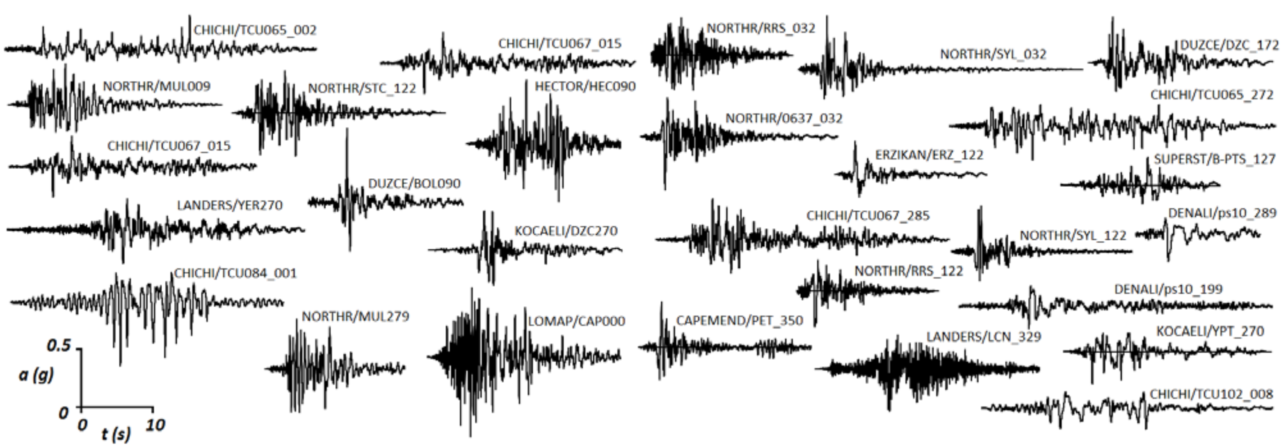

Fig. 2 – Ground acceleration histories of the normalized records

Fig. 3 displays 5% damped elastic pseudo-acceleration response spectra (PSa). Computed PSa envelope, mean PSa, standard deviation (σ) and reference spectrum for soil class III in seismic zone of very high seismic hazard according to categorization of Iranian seismic design guidelines Standard 2800 [19] are presented in this figure. Generated ground motions spectra displayed in Fig. 3 is compared to the Iranian seismic design spectrum (Standard 2800). Spectral ordinates of mean spectrum for periods around T_1=1.35 s approximately coincide with those of the design spectrum. For periods other than 1.35 s, spectral ordinates are in general slightly less than those of the design spectrum.

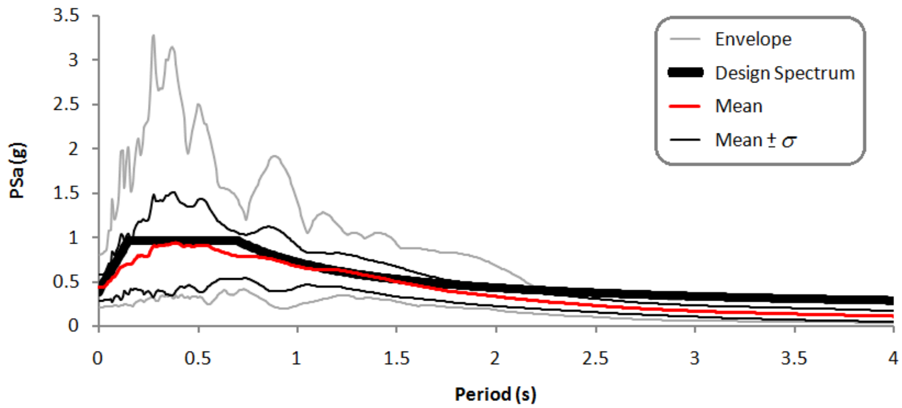

Fig. 3 – Scaling of the normalized records based on the Iranian seismic design spectrum (Standard 2800)

5. Dynamic time-history analyses

Consider the 5-story steel MRF structure as described in section 2. The boundary condition of the structure is assumed to be (i) fixed base, (ii) linear SSI and uncoupled foundation (i.e. without tie beams), (iii) nonlinear SSI and uncoupled foundation, and (iv) nonlinear SSI and coupled foundation (i.e. with tie beams). These boundary conditions are denoted by Case 1 through 4, in the same order. The seismic performance of the four alternatives is investigated through NTHAs. An ensemble of 27 real accelerograms is used as seismic excitation of the soil-foundation-structure system, as described in previous section. In all cases, the seismic excitation is applied at the far ends of the zero-length elements at the boundaries, as displayed schematically in Fig. 1b.

In the following, the SSI effects on displacement as well as force demands of the superstructure are typically investigated when the soil-foundation-structure system is subjected to an individual ground motion.

5.1 SSI effects on force demands

The SSI effect on force demands of the building is investigated at two different excitation levels. Normalized base shear, defined as base shear divided by total weight of the superstructure, is selected as quantitative index of the structural force demands. The two excitation levels are selected as design basis earthquake (DBE) and maximum credible earthquake (MCE). The latter is defined as 1.5 times the DBE excitation level.

As an example, the normalized base shear histories are plotted in Fig. 4 when the frame is typically subjected to fault-normal component (ps10_199) of 2002 Denali, Alaska, TAPS Pump Sta. #10 ground motion. The time history of ground velocity is shown in Fig. 4a. The Arias intensity of the record is displayed in Fig. 4b to represent the rate of seismic input energy to the soil-foundation-structure system. The normalized base shear histories in cases 1 and 4 are given in Figs. 4c and 4d, respectively. The normalized base shear histories are plotted in pair corresponding to DBE (in black) as well as MCE (in red) excitation levels. The results show that the force demands are reduced in nonlinear SSI condition (case 4) especially at DBE level. So that the maximum absolute value of normalized base shear at DBE level is 0.301 in case 1 which is reduced to 0.263 in case 4. But the base shear is slightly reduced at MCE level. Overall, the results show that the SSI effects on force demands are not of great importance according to this individual NTHA.

Bearing in mind that the spectral acceleration SA of a motion is not always the most crucial parameter of nonlinear response, the characterization of the seismic motions with respect to the exceedence of the design limits is conducted on the basis of spectral displacements SD, following the logic of displacement-based design [e.g. 20-22]. Accordingly, the SSI effects on displacement demands of the superstructure are discussed in the following section.

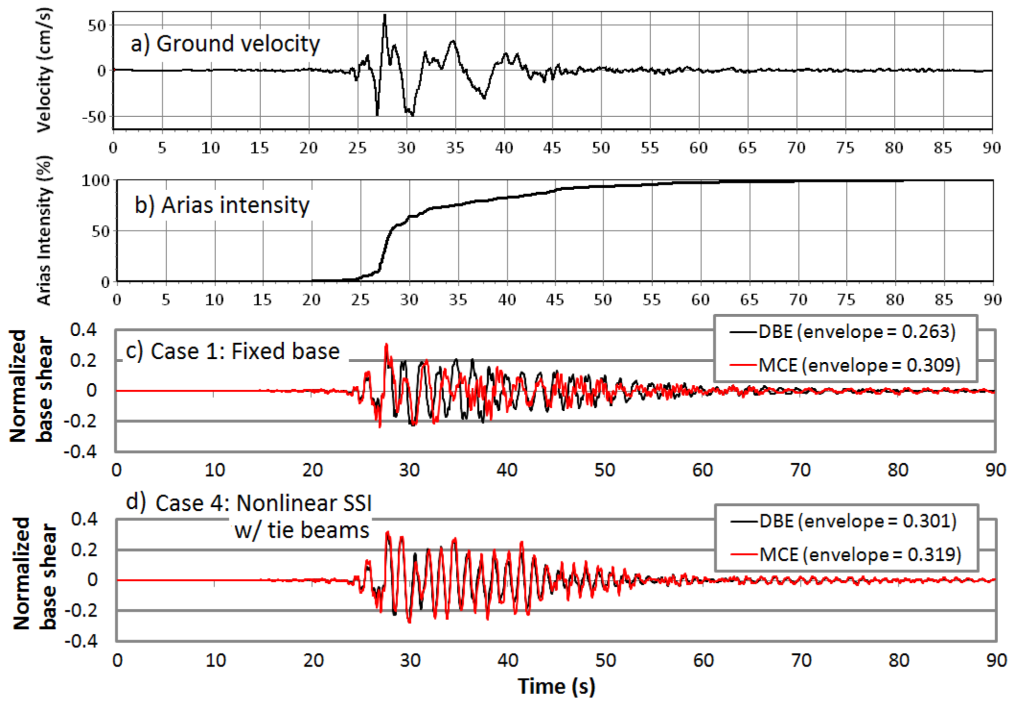

Fig. 4 – Time-history of normalized base shear in two different SSI conditions

5.2 SSI effects on displacement demands

The SSI effect on displacement demands of the building is investigated at DBE and MCE excitation levels. Interstory drift ratio (IDR), defined as the envelope of relative displacement between two consecutive story levels normalized by the story height, is used as the primary engineering demand parameter. In order to estimate the relative IDRs, the rigid-body interstory displacements caused by rocking behavior of the frame are extracted in cases 2 through 4. For this purpose, the average foundation tilting angles are computed among the four footings.

Fig. 5 illustrates the distribution of IDRs over the height for the four SSI cases comparatively. The soil-structure system is subjected to fault-normal component (ps10_199) of 2002 Denali, Alaska, TAPS Pump Sta. #10 ground motion. The incident record is scaled to DBE (not exceeding design limits) as well as MCE (exceeding design limits) as given in Figs. 5a and 5b, respectively.

The results of Fig. 5a show that nonlinear SSI during the selected earthquake not exceeding design limits leads to significant reduction in drift demands especially in middle stories. In contrast, the IDRs in case 3 are increased in lower stories so that the IDR of the base is significantly greater than cases 1 and 2. Meanwhile, the coupled performance of foundation with tie beams in case 4 at DBE level has noticeably improved the drift demands at lower stories i.e. IDR equal to 0.022 in case 3 is reduced to 0.011 in case 4.

Fig. 5b shows that the gap between IDRs in cases 3 and 4 compared to cases 1 and 2 is widened when the excitation is intensified up to MCE, especially in lower stories. Evidently, the IDR is more uniformly distributed along height when nonlinear SSI is incorporated. Yet, infinitesimal difference is observed between case 4 compared to case 3 which indicates that the superstructure’s displacement demands are almost independent of the tie beams.

According to the thresholds introduced in HAZUS [2] for moderate-code mid-rise steel moment frames (S1M), the IDR equal to 0.0157 and 0.04 is corresponding to extensive as well as complete structural damage states, respectively. Then, with regard to the typical results of Fig. 5b it is demonstrated that the damage state of the superstructure from complete structural damage state in cases 1 and 2 is lowered to extensive damage in cases 3 and 4. This fact reveals the significant role of nonlinear SSI incorporation on seismic damage of the superstructure during earthquakes exceeding design limits. In addition, based on the obtained typical results, application of tie beams is another key factor which can affect the damage state of the building during earthquakes not exceeding design limits.

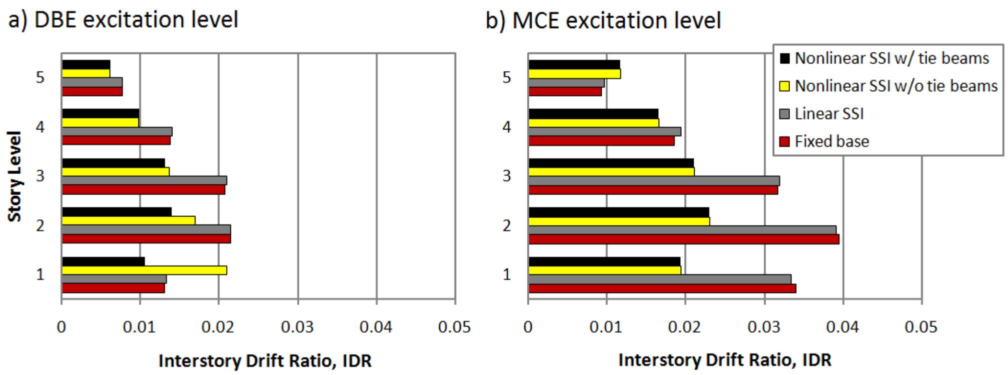

Fig. 5 – SSI effects on drift demands at two different excitation levels

Based on the observations, the nonlinear SSI incorporation and coupled performance of the foundation system due to tie beams are the two key factors which can potentially influence the estimated seismic damage of a building subjected to a given ground motion. Hence, these two factors are investigated in the NTHA-based fragility analysis of the steel frame in this study.

6. Fragility curves of the steel frame

Assuming that the 27 real ground motions provide enough information to reliably estimate the parameters defining the fragility curve, the IDA analysis data are generated in the four cases, as introduced in section 5, comparatively. As a matter of fact, the rocking motions of the footings are not identical at a given arbitrary moment. This fact biases the damage estimation based exclusively on interstory drifts especially at strong excitation levels while the structure is prior to collapse. To solve this problem, a different damage measure is applied in this study which is based on moment-rotation hysteresis loops in plastic hinges.

6.1 Damage measure

Different types of damage models have been introduced by researchers in the last few decades. Considering realistic prediction of actual damage states as well as wide applicability to RC, steel [23,24] and timber [25] structures, in addition to compatibility with different hysteresis characteristics, the Park-Ang model is one of the most preferable choices as a structural damage index.

The structural damage based on Park-Ang model, is a function of (i) the response i.e. maximum deformation of structure during an earthquake and hysteretic energy absorbed by building structure during NTHA that are both dependent on the loading history, and (ii) the parameters that specify the structural capacity. Values of the Park-Ang damage index greater than unity signifies collapse or total damage of the structure [26].

As a next step in the process of damage analysis, the calculated Park-Ang damage indices, denoted by DI_{PA}, should be related to some predefined damage states leading to an estimation of economic losses imposed on the structures. For this purpose, the following damage states are defined: (i) $DI_{\mathrm{PA}} \leq 0.2$ representing Slight damage, (ii) $0.2 \leq DI_{\mathrm{PA}} \leq 0.4$ representing Moderate (repairable) damage, (iii) $0.4 \leq DI_{\mathrm{PA}} \leq 1.0$ representing Extensive damage (beyond repair), and (iv) $1.0 \leq DI_{\mathrm{PA}}$ representing loss of the structural component.

The Park-Ang damage index DI_{PA} can be obtained for an individual structural member (local damage index), for each story of the building (story damage index), and for the whole of the structure (global damage index). The story damage index, story DI_{PA}, and global damage index, *Global* DI_{PA}, can be calculated as the weighted average of the local damage indices while the maximum total energy absorbed by each element would be weighting factor. In this study, the global damage indices are calculated for overall structural damage assessment purposes.

6.2 SSI effects on local as well as global damage indices

Consider the 5-story steel MRF structure as described in section 2. As an illustrative example, the damage distribution within the frame is shown in Fig. 6 when the frame is typically subjected to fault-normal component (ps10_199) of 2002 Denali, Alaska, TAPS Pump Sta. #10 ground motion. The incident record is scaled to MCE (exceeding design limits). The SSI boundary conditions are denoted by cases 1 through 4 in Fig. 6, as introduced in section 5. A color spectrum is introduced to represent the local damage index of each member in Fig. 6. The global damage indices of each structure are also presented in Fig. 6. The moment-rotation history of a typical member is depicted in Fig. 7. These M-θ loops belong to left-end plastic hinge of the interior beam at first floor as a representative structural member. As shown, the internal area of the loops is limited in nonlinear SSI condition. It is obvious that the nonlinear SSI has significantly reduced the damage state of the structure. On the other hand, damage state of the superstructure is enhanced when the footings are coupled (i.e. tie beams are used), so that the *Global* DI_{PA} is reduced from 0.877 in case 3 to 0.560 in case 4, according to Fig. 6.

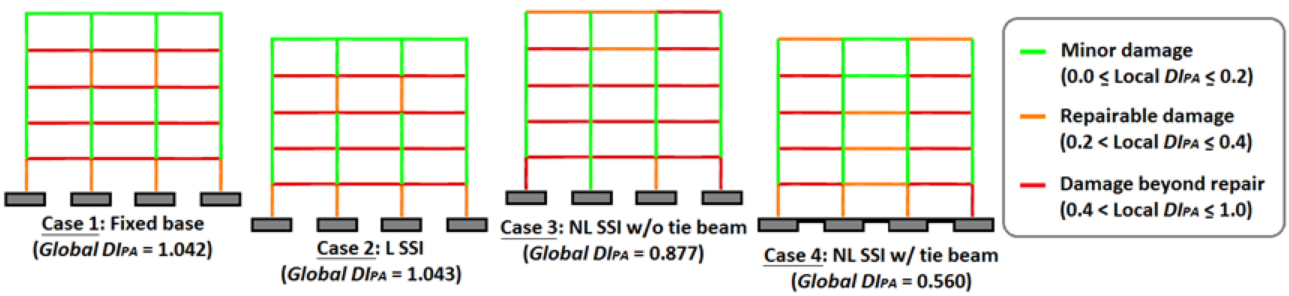

Fig. 6 – Typical distribution of local damage indices over the structural members

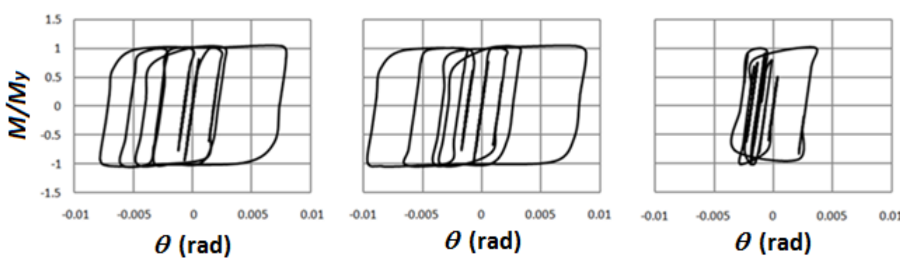

Fig. 7 – Moment-rotation hysteresis loops at left-end plastic hinge of a typical beam member: a) Fixed-base (case 1), b) Linear SSI (case 2), and c) Nonlinear SSI without tie beams (case 3).

Comparing the damage indices shows that the beams which are responsible for structural energy dissipation of the MRF structure are significantly protected when nonlinear SSI is included, so that benefiting from rocking isolation effects the irreparable damages in critical members of the fixed-base frame are lowered close to minor damage limit. In contrary, linear SSI (case 2 in Fig. 6), which means flexible-base foundation without uplifting and soil yielding, has a negligible contribution to the problem and does not attract attention as a key issue.

6.3 Extracting fragility curves from IDA results

A fragility function specifies the probability of collapse, or some other limit state of interest, of a structure as a function of some ground motion intensity measure, *IM*. The parameter *IM* is often quantified by spectral acceleration with a specified period and damping, though any measure of ground motion intensity can be used with the procedures below. Collapse fragility functions obtained from structural analysis results are increasingly popular in structural assessment procedures [17,27].

For a given ground motion and dynamic structural analysis result, the occurrence or nonoccurrence of collapse can be defined in a number of ways [28]. In this paper it is assumed that comparing *Global* DI_{PA} to threshold 1.0 determines whether or not the ground motion caused collapse. The results below are not limited to collapse level only, and in fact any performance level of interest is assessed using its corresponding damage state according to thresholds given in Section 6.1.

There are a number of procedures for performing nonlinear dynamic structural analyses to collect the data for estimating a fragility function. One common approach is incremental dynamic analysis (IDA), where a suite of ground motions are repeatedly scaled in order to find the *IM* level at which each ground motion causes collapse [29,17]. For fragility function fitting, an optimal strategy, as described below, must be followed in order to obtain an accurate fragility estimate with a minimal number of structural analyses.

In the case of analytical fragility functions, a lognormal cumulative distribution function is often used to define a fragility function

$$P(C \mid IM = x) = \Phi\left(\frac{\ln(x/\theta)}{\beta}\right) \tag{1}$$

where $P(C \mid IM = x)$ is the probability that a ground motion with $IM = x$ will cause the structure to collapse, $\Phi(\ )$ is the standard normal cumulative distribution function (CDF), θ is the median of the fragility function (the *IM* level with 50% probability of collapse) and β is the standard deviation of ln*IM* (sometimes referred to as the dispersion of *IM*). Equation 1 implies that the *IM* values of ground motions causing collapse of a given structure are log-normally distributed. Calibrating equation 1 for a given structure requires estimating θ and β from structural analysis results. We denote estimates of those parameters as $\hat{\theta}$ and $\hat{\beta}$.

Parameter estimation is the field of statistics associated with estimating values of model parameters based on observed data that has a random component. In this case, our parameters of interest are θ and β, and we have randomness because record-to-record variability causes ground motions with the same *IM* level to produce different demands on a given structure. There are a number of ways to estimate parameter values for a fragility function that are consistent with observed data, depending upon the procedure used to obtain structural analysis data. IDA is the procedure used in this study to obtain the analysis data.

Incremental dynamic analysis (IDA) involves scaling each ground motion in a suite until it causes collapse of the structure [29]. This process produces a set of *IM* values associated with the onset of collapse for each ground motion.

The probability of collapse at a given *IM* level, *x*, can then be estimated as the fraction of records for which collapse occurs at a level lower than *x*. Fragility function parameters can be estimated from this data by taking logarithms of each ground motion's *IM* value associated with onset of collapse, and computing their mean and standard deviation, as follows:

$$\ln\hat{\theta} = \frac{1}{n}\sum_{i=1}^{n}\ln IM_i \tag{2}$$

$$\hat{\beta} = \sqrt{\frac{1}{n-1}\sum_{i=1}^{n}\left(\ln\left(IM_i/\hat{\theta}\right)\right)^2} \tag{3}$$

where n is the number of ground motions considered, and IM_i is the *IM* value associated with onset of collapse for the ith ground motion. This is a method of moments estimator, as $\ln\theta$ and β are the mean and standard deviation, respectively, of the normal distribution representing the ln*IM* values. Note that the mean of ln*IM* is equal to the median of *IM* in the case that *IM* is lognormally distributed, which is why using the sample mean in this manner produces an estimate of θ. The mean and standard deviation, or moments, of the distribution are estimated using the sample moments from a set of data. Fragility function fitted using this approach are shown in Fig. 8 for fixed-base structure (case 1) as well as nonlinear SSI condition and coupled foundation (case 4). These damage states are derived for the highest damage state corresponding to *Global* $DI_{\mathrm{PA}} \geq 1.0$ which represents building collapse.

6.4 Fragility curves at different damage states

The fragility curves for the first to fourth damage states (i.e. Slight, Moderate, Extensive, and Complete damage as introduced in section 6.1) are computed while the different SSI boundary conditions are compared. The derived fragility curves are presented in Fig. 9. Evidently, the fragility curves agree with the tendencies of the dynamical responses as described in section 5, i.e. a general reduction is observed when nonlinear SSI effects are included. This reduction of the structural demand is related to the combined effect of radiation damping, modification of vibrating modes and hysteretic damping of soil due to its nonlinear behavior i.e. foundation uplifting and soil yielding. Concerning the Slight damage state, a reduction of near to 50% of the probability to reach this damage state is obtained for motion with $S_a(T_1) < 0.5$g. This difference decreases gradually as the severity of the motion increases. Regarding the Moderate state level, the fragility curves start approximately at $S_a(T_1) = 0.6$g, nevertheless the probability to reach the Moderate damage state is reduced up to 40% when nonlinear SSI effects are included in the analysis. This difference decreases gradually for motions with $S_a(T_1) = 2.0$g. In this case, SSI effects are still favorable to reduce seismic demand under Moderate damage state threshold at strong motions. At Extensive damage state level, the fragility curves start approximately at $S_a(T_1) = 0.8$g. The probability to reach the Extensive damage state is reduced up to 45% when nonlinear SSI effects are included. This difference decreases gradually for motions with $S_a(T_1) = 2.7$g. At the highest damage state, namely Complete damage, the fragility curves start approximately at $S_a(T_1) = 1.2$g. The probability to reach the Complete damage state is reduced up to 10% when nonlinear SSI effects are included and the foundation is uncoupled. This reduction is even intensified in nonlinear SSI condition while the foundation is integrated with tie beams. In such condition, thank to application of tie beams, the greatest beneficial effects (up to 20%) on enhancing the seismic demands are captured under Complete damage state threshold.

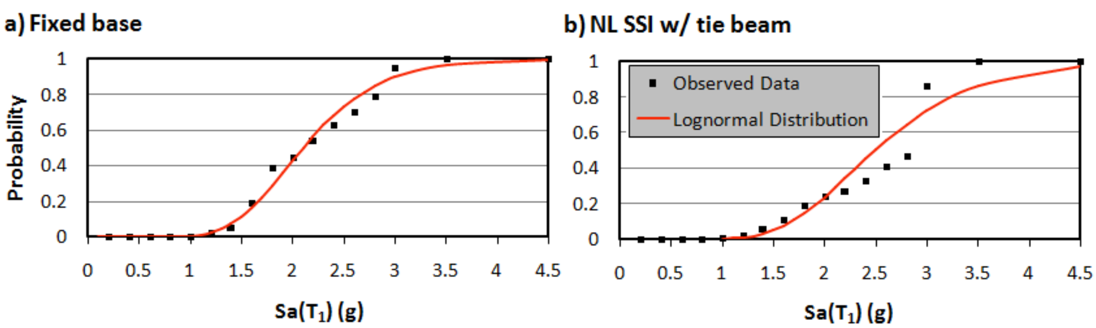

Fig. 8 – Extracting fragility curves with the best fit to the statistical data points (two different SSI conditions are compared for illustrative purposes)

In a statistical context, the agreement between the fragility curves derived for the example building studied in this paper are quite satisfactory. As expected, the derived fragility curves provide a reliable quantification of the effects of the nonlinear SSI on the seismic vulnerability assessment of the considered building. Further investigations in this way will be needed in order to obtain more general conclusions for diverse building typologies, foundation systems and soil types.

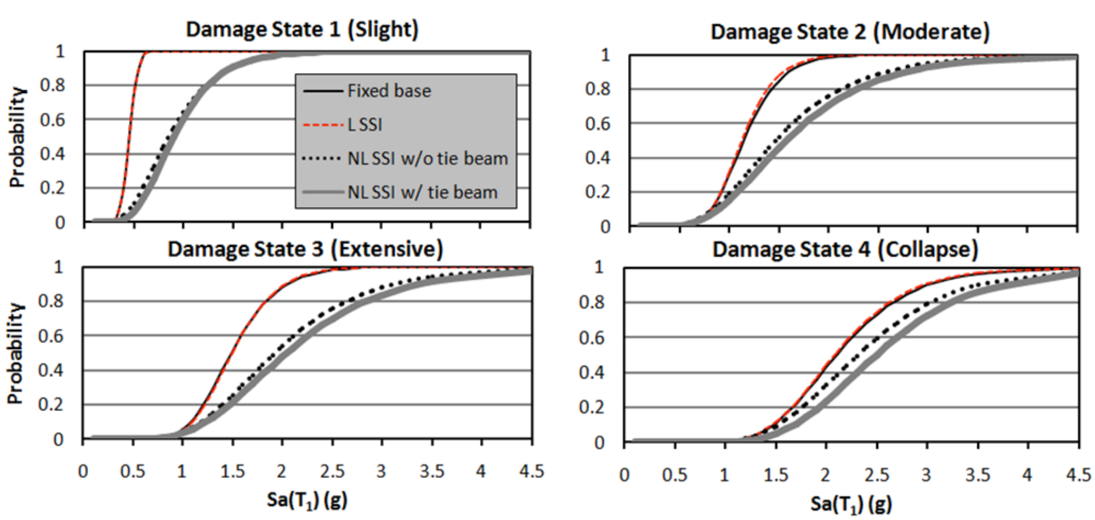

Fig. 9 – Computed fragility curves at different damage states as well as different SSI conditions

7. Conclusions

A study on the influence of nonlinear SSI on the assessment of the seismic vulnerability of steel buildings is presented in this paper. Two major aspects have been exposed. The first refers to the effects of foundation uplifting and soil yielding by which the plastic hinge formation would be invited within the underlying soil and consequently the superstructure remains protected. The second examines the role of foundation system in NTHA-based damage estimation. To this end, application of tie beams is evaluated and two sets of fragility curves are compared at different damage states. The modeling of nonlinear SSI is performed using the modified Beam-on-Nonlinear Winkler Foundation (BNWF). The constructed model is accurate enough for practical purposes and provides an important economy in time and CPU consumption compared to direct approach. The fragility curves are developed to summarize results from dynamic time history analyses.

According to the findings of this study, there is a reduction in seismic demands in general when nonlinear SSI is included. This reduction can be associated fundamentally with two phenomena: radiation damping and hysteretic damping due to foundation uplifting and soil yielding. Evidently, the results of some existing time-history analyses performed in this study manifest unexpected increases in structural demands. Accordingly, it might be early to over-generalize the observations. A set of modified fragility curves dealing with SSI effects are derived by which more realistic seismic loss estimations would be possible. These modification factors need to be generalized with respect to diverse structure, foundation, and soil typologies.

8. Acknowledgements

This research is financially supported by Road, Housing, and Urban Development Research Center which is gratefully acknowledged.

9. References

[1] Applied Technology Council (1985): Earthquake damage evaluation data for California. Report ATC-13, Redwood City, CA,.

[2] Federal Emergency Management Agency (2003): Multi-hazard loss estimation methodology. Earthquake model, HAZUSMHMR1 Technical Manual, Washington DC.

[3] Song J, Ellingwood BR (1999): Probabilistic modeling of steel moment frames with welded connections. *Engineering Journal (AISC)*, **36** (3), 129-137.

[4] Kwon OS, Elnashai A (2006): The effect of material and ground motion uncertainty on the seismic vulnerability curves of RC structure. *Engineering Structures*, **28** (2), 289-303.

[5] Ellingwood BR, Celik OC, Kinali K (2007): Fragility assessment of building structural systems in Mid-America. *Earthquake Engng & Struct. Dyn.*, **36**, 1935-1952

[6] Sáez S, Lopez-Caballero F, Modaressi-Farahmand-Razavi A (2011): Effect of the inelastic dynamic soil-structure interaction on the seismic vulnerability assessment. *Structural Safety*, **33**, 51-63.

[7] ASCE 7-10 (2010): Minimum Design Loads for Buildings and Other Structures. American Society of Civil Engineers, Reston, Virginia.

[8] American Institute of Steel Construction (2005): Specification for Structural Steel Buildings. Chicago, IL.

[9] Pacific Earthquake Engineering Research Center, PEER (2008): Open system for earthquake engineering simulation (OpenSees), http://opensees.berkeley.edu/.

[10] Ibarra LF, Krawinkler H (2005): Global collapse of frame structures under seismic excitations. Rep. No. TB 152, The John A. Blume Earthquake Engineering Center, Stanford University, Stanford, CA.

[11] Lignos DG, Krawinkler H (2011): Deterioration modeling of steel components in support of collapse prediction of steel moment frames under earthquake loading. *Journal of Structural Engineering, ASCE*, **137** (11), 1291-1302.

[12] Gajan S, Raychowdhury P, Hutchinson TC, Kutter BL, Stewart JP (2010): Application and Validation of Practical Tools for Nonlinear Soil-Foundation Interaction Analysis. *Earthq. Spectra*, **26** (1), 111-129.

[13] Harden CW, Hutchinson TC (2009): Beam-on-nonlinear-Winkler-foundation modeling of shallow, rocking-dominated footings. *Earthquake Spectra*, **25** (2), 277-300.

[14] Harden CW, Hutchinson T, Martin GR, Kutter BL (2005): Numerical modeling of the nonlinear cyclic response of shallow foundations. Report No.PEER-2005/04, Pacific Earthquake Engineering Research Center, University of California, Berkeley.

[15] Raychowdhury P, Hutchinson TC (2008): Nonlinear material models for Winkler-based shallow foundation response evaluation. *Proc. of GeoCongress: Characterization, Monitoring, and Modeling of GeoSystems*, New Orleans, LA, 686-693.

[16] Gajan S, Hutchinson TC, Kutter BL, Raychowdhury P, Ugalde JA, Stewart JP (2008): Numerical Models for Analysis and Performance-Based Design of Shallow Foundations Subjected to Seismic Loading. PEER Report 2007/04, Pacific Earthquake Engineering Research Center College of Engineering, UC Berkeley.

[17] Federal Emergency Management Agency, FEMA (2009): Quantification of building seismic performance factors, FEMA P695. Washington DC.

[18] Baker JW (2007): Quantitative classification of near-fault ground motions using wavelet analysis. *Bulletin of Seismological Society of America*, **97** (5), 1486-501.

[19] Iranian Code of Practice for Seismic Resistant Design of Buildings, Standard No. 2800 (2014) Road, Housing, and Urban Development Research Center, 4th edition.

[20] Bertero V (1996): State of the art report on: design criteria. *Proceedings of 11th world conference on earthquake engineering*, Acapulco, Mexico, Oxford, Pergamon.

[21] Tassios TP (1998): Seismic design: state of practice. *Proceedings of 11th european conference on earthquake engineering*, Rotterdam, AA Balkema, 255-267.

[22] Priestley MJN (2000): Performance based seismic design. *Proc. 12th world conference on earthquake engineering (12WCEE)*, Auckland, New Zealand, Paper No. 2831.

[23] Park YJ, Ang AH, Wen YK (1987): Damage-limiting aseismic design of buildings. *Earthquake Spectra*, **3** (1), 1-26.

[24] Ghosh S, Datta D, Katakdhond AA (2011): Estimation of the Park-Ang damage index for planar multi-storey frames using equivalent single-degree systems. *Engineering Structures*, **33**, 2509-2524.

[25] Van de Lindt JW (2005): Damage-based seismic reliability concept for woodframe structures. *J Struct Eng, ASCE*, **131** (4), 668-75.

[26] Park YJ, Ang AH (1985) Mechanistic Seismic Damage Model for Reinforced Concrete. *Journal of Structural Engineering, ASCE*, **111** (4), 722-739.

[27] Applied Technology Council (2012): ATC-58, Seismic Performance Assessment of Buildings. Redwood City, California.

[28] Zareian F, Krawinkler H (2007): Assessment of probability of collapse and design for collapse safety. *Earthquake Engineering & Structural Dynamics*, **36** (13), 1901-1914.

[29] Vamvatsikos D, Cornell CA (2002): Incremental dynamic analysis. *Earthquake Engineering & Structural Dynamics*, **31** (3), 491-514.